

Resonant inelastic X-ray scattering of a Ru photosensitizer: Insights from individual ligands to the electronic structure of the complete molecule

Cite as: J. Chem. Phys. **151**, 074701 (2019); <https://doi.org/10.1063/1.5114692>

Submitted: 11 June 2019 . Accepted: 25 July 2019 . Published Online: 19 August 2019

Robert H. Temperton , Stephen T. Skowron , Karsten Handrup, Andrew J. Gibson , Alessandro Nicolaou, Nicolas Jaouen , Elena Besley , and James N. O'Shea 



View Online



Export Citation



CrossMark

ARTICLES YOU MAY BE INTERESTED IN

[Modular path integral for discrete systems with non-diagonal couplings](#)

The Journal of Chemical Physics **151**, 074110 (2019); <https://doi.org/10.1063/1.5108692>

[Intra-dimer row and inter-dimer row coupling of the vibrational modes of chemisorbed CO on Si\(001\)-c\(4 × 2\) observed by angle-dependent transmission infrared spectroscopy](#)

The Journal of Chemical Physics **151**, 074702 (2019); <https://doi.org/10.1063/1.5109950>

[Contributions of force field interaction forms to Green-Kubo viscosity integral in n-alkane case](#)

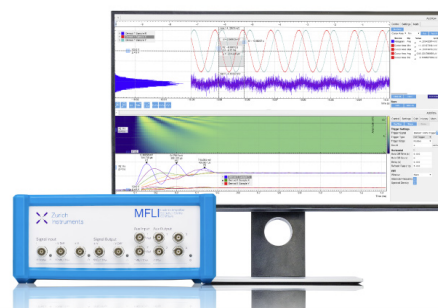
The Journal of Chemical Physics **151**, 074502 (2019); <https://doi.org/10.1063/1.5103265>

Challenge us.

What are your needs for periodic signal detection?



Zurich
Instruments



Resonant inelastic X-ray scattering of a Ru photosensitizer: Insights from individual ligands to the electronic structure of the complete molecule

Cite as: J. Chem. Phys. 151, 074701 (2019); doi: 10.1063/1.5114692

Submitted: 11 June 2019 • Accepted: 25 July 2019 •

Published Online: 19 August 2019



View Online



Export Citation



CrossMark

Robert H. Temperton,¹ Stephen T. Skowron,² Karsten Handrup,³ Andrew J. Gibson,¹ Alessandro Nicolaou,⁴ Nicolas Jaouen,⁴ Elena Besley,² and James N. O'Shea^{1,a)}

AFFILIATIONS

¹School of Physics and Astronomy, University of Nottingham, Nottingham, NG7 2RD, United Kingdom

²School of Chemistry, University of Nottingham, Nottingham, NG7 2RD, United Kingdom

³Synchrotron Radiation Research, Department of Physics, Box 118, SE-221 00 Lund, Sweden

⁴Synchrotron SOLEIL, Saint-Aubin, BP 48, 91192 Gif-sur-Yvette, France

^{a)}Electronic mail: J.Oshea@nottingham.ac.uk

ABSTRACT

N 1s Resonant Inelastic X-ray Scattering (RIXS) was used to probe the molecular electronic structure of the ruthenium photosensitizer complex *cis*-bis(isothiocyanato) bis(2,2'-bipyridyl-4,4'-dicarboxylato) ruthenium(II), known as "N3." In order to interpret these data, crystalline powder samples of the bipyridine-dicarboxylic acid ligand ("bi-isonicotinic acid") and the single ring analog "isonicotinic acid" were studied separately using the same method. Clear evidence for intermolecular hydrogen bonding is observed for each of these crystalline powders, along with clear vibronic coupling features. For bi-isonicotinic acid, these results are compared to those of a physisorbed multilayer, where no hydrogen bonding is observed. The RIXS of the "N3" dye, again prepared as a bulk powder sample, is interpreted in terms of the orbital contributions of the bi-isonicotinic acid and thiocyanate ligands by considering the two different nitrogen species. This allows direct comparison with the isolated ligand molecules where we highlight the impact of the central Ru atom on the electronic structure of the ligand. Further interpretation is provided through complementary resonant photoemission spectroscopy and density functional theory calculations. This combination of techniques allows us to confirm the localization and relative coupling of the frontier orbitals and associated vibrational losses.

Published under license by AIP Publishing. <https://doi.org/10.1063/1.5114692>

I. INTRODUCTION

Ruthenium centered organometallic complexes have a range of applications in light harvesting devices such as dye sensitized solar cells (DSSCs)¹ and photoelectrochemical water splitting devices.² This study is focused on the "N3" dye, *cis*-bis(isothiocyanato) bis(2,2'-bipyridyl-4,4'-dicarboxylic acid) ruthenium(II) also known as Ru535, which has become a benchmark molecule for use in DSSCs and has been previously studied using photoelectron spectroscopies on rutile titanium dioxide,³ gold,^{4,5} and aluminum oxide

surfaces.⁶ N3 bonds to oxide surfaces primarily through the carboxyl groups of the bi-isonicotinic acid (2,2'-bipyridyl-4,4'-dicarboxylic acid) ligands, which in turn is made up of two isonicotinic acid molecules (pyridine-4-carboxylic acid). These molecules, shown in Fig. 1(a), are also well-studied, where bi-isonicotinic acid, in particular, has proven to act as a model system of these dye sensitized devices, allowing investigation of the absorption, bonding, and charge transfer dynamics between the ligand and surface.⁷⁻¹¹

X-ray photoelectron spectroscopy (XPS) and X-ray absorption spectroscopy (XAS) highlight an interesting difference between

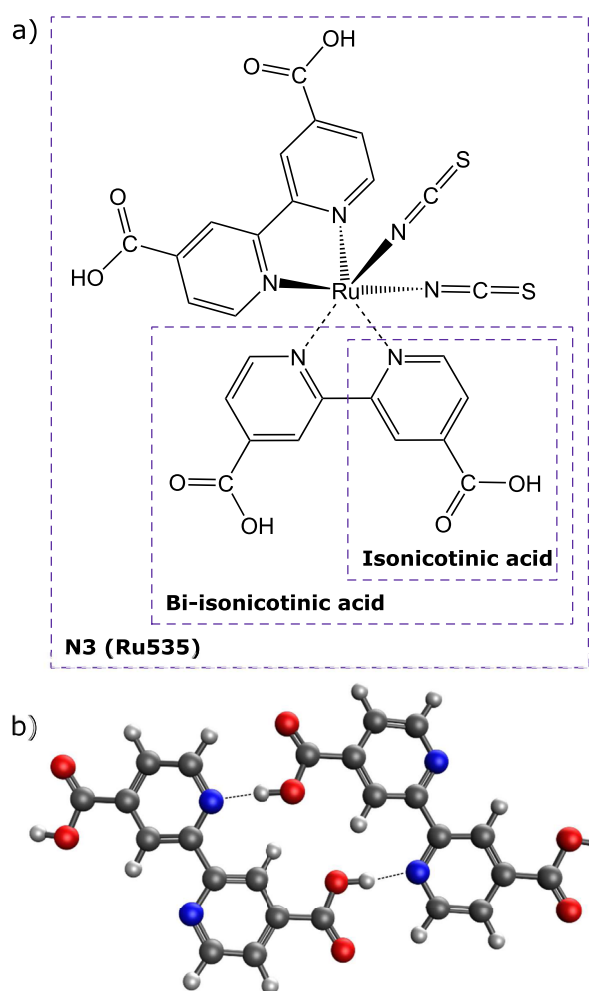


FIG. 1. (a) Schematic illustration of the chemical structures of the N3 dye complex, its bi-isonicotinic acid ligand, and the single pyridine ring analog isonicotinic acid. (b) Calculated geometry of the hydrogen-bonding motif of bi-isonicotinic acid known from X-ray diffraction to be present in the crystal structure.¹²

the isonicotinic acid and bi-isonicotinic acid molecules with regard to the head-to-tail hydrogen bonding between the N atom of the pyridine ring and the OH group of the carboxyl group of neighboring molecules. For multilayers of isonicotinic acid, hydrogen bonding has been shown to produce a core level shift in the XPS and an additional state in the XAS.^{13,14} For bi-isonicotinic acid, we believe that no conclusive evidence of hydrogen bonding has been observed for multilayers of the molecule on a surface despite the fact that in the bulk crystal structure, each carboxylic acid group is hydrogen bonded to the pyridine nitrogen in a neighboring molecule, as illustrated in Fig. 1(b). In this crystal structure, the bi-isonicotinic acid molecules are arranged in two-dimensional sheets participating in both head-to-tail hydrogen bonding and face-to-face π - π interactions.¹² Similarly, the crystal structure of

isonicotinic acid shows linear chains of head-to-tail hydrogen-bonded molecules.¹⁵

Resonant inelastic X-ray scattering (RIXS) can provide atom-specific information about the occupied and unoccupied valence orbitals of a molecule and the coupling between them.¹⁶ It is therefore an ideal probe of the molecular electronic structure, which underpins electron dynamics and thus solar energy conversion mechanisms in molecular systems.¹⁷ RIXS also provides a sensitive probe of molecular interactions such as hydrogen-bonding.^{18,19} In RIXS, the unoccupied molecular orbitals are populated by excitation of a core-electron through the absorption of a photon tuned to a specific resonance producing a core-excited state. The de-excitation step proceeds either from the populated state (elastic scattering and any vibrational losses) or from an occupied valence state (inelastic scattering). The inelastic scattering projects the partial density of valence states onto the core-level and is governed by the dipole selection rule. In our case, by tuning the absorption energy for excitation of an N 1s electron into the lowest unoccupied molecular orbitals (LUMOs) of each molecule, we therefore probe the unoccupied N 2p-derived orbitals.

In this paper, we present two-dimensional N 1s RIXS maps of isonicotinic acid, bi-isonicotinic acid, and N3 in their bulk crystalline form. This represents a systematic increase in complexity from the simplest pyridine carboxylic acid ligand to the ruthenium dye complex. We aim to use these data to investigate the similarities and differences in the electronic structure of the ligands in isolation and as part of the N3 complex allowing us to comment on the appropriateness of using individual ligand molecules as an analog for the complete complex. For bi-isonicotinic acid, we compare the bulk crystalline powder RIXS to that of a thick multilayer film physisorbed on a surface to highlight differences in the intermolecular interactions in these two phases. Specifically, we discuss an additional resonant transition only observed in the presence of hydrogen-bonding. For N3, we interpret the RIXS in terms of a projection of the valence structure onto the two distinct nitrogen species in the molecule. Finally, we compare this to resonant photoemission electron spectroscopy (RPES), which is the nonradiative complement to RIXS that also allows observation of the coupling between occupied and unoccupied states. This aids our assignments of the valence features and resonant transitions to occupied and unoccupied frontier molecular orbitals determined by density functional theory calculations.

II. METHODS

A. Experimental

N 1s Resonant Inelastic X-ray Scattering (RIXS) measurements were performed using the AERHA (adjustable energy resolution high acceptance) spectrometer²⁰ at the Sextants beamline²¹ at Synchrotron SOLEIL in France. Bulk/powder samples were made by pressing the bulk crystalline powder of N3 (Solaronix), bi-isonicotinic acid (Alfa Aesar), and isonicotinic acid (Sigma Aldrich) onto a graphite tape. Multilayer bi-isonicotinic acid samples were prepared on rutile TiO₂(110) single crystal surfaces (Pi-Kem, UK) in a separate ultrahigh vacuum (UHV) system in our home laboratory, equipped with a Scienta R3000 analyzer and dual anode (Al K α and Mg K α) X-ray source. The TiO₂(110) was

cleaned by repeated cycles of argon ion sputtering (2 kV followed by 1 kV and annealing in UHV to ~ 900 K until no C 1s signal was detected in the XPS). Multilayers of bi-isonicotinic acid were then deposited onto the TiO₂, held at room temperature, by sublimation from a Knudsen-type cell evaporation source (at ~ 500 K) until no Ti 2p signal was detected in the XPS. The multilayer samples were then transported to SOLEIL in air and transferred into the analysis chamber of the Sextants beamline where the base pressure was 1×10^{-8} mbar. The RIXS measurements were not sensitive to surface contamination from the atmosphere as RIXS, a bulk sensitive technique, was performed at the nitrogen edge.

The incident beam at Sextants is focused to a spot size of $2(v) \mu\text{m} \times 100(h) \mu\text{m}$. To prevent beam damage of the molecules, the sample was continuously moved during the measurements at a rate such that no changes were observed in concurrent spectra. The emitted photon energy scale of the RIXS spectrometer was calibrated by measuring the elastic peak at 5 eV increments across the whole detector range using linear vertical polarization of the incoming beam to maximize the elastic (Rayleigh) scattering intensity. For the RIXS maps and XAS over the N 1s absorption edge, the beam was linearly polarized in the horizontal plane (in the plane of the spectrometer) and an incidence angle of 35° with respect to the surface. The scattering angle was set to 85° . The overall measurement resolution was set to 300 meV (compared to the optimum resolution of 110 meV) as a compromise between energy resolution and spectrometer transmission. The RIXS maps are constructed from X-ray emission spectra measured for 10 min at each absorption energy.

Resonant photoemission spectroscopy (RPES) of N3 was carried out at beamline I511 on the MAX-II ring at the former MAX-Lab synchrotron radiation facility (now MAX-IV). These previously unpublished data were collected as part of the study presented by Mayor *et al.* in 2008³ where details about the measurements can be found with the exception that the multilayer N3 sample was prepared *ex situ* by electro spray deposition²² in low vacuum (whereas Mayor's paper presents *in situ* deposits in high vacuum). Further information about the electro spray deposition can be found elsewhere.²² Again, a rutile TiO₂(110) single crystal was used as a substrate prepared as described above prior to being removed from the UHV preparation chamber for the deposition. After the deposition, the sample was transferred immediately back into the UHV system for the measurements.

B. Computational

Density functional theory (DFT) calculations were performed using the Q-Chem 5.0 quantum chemistry software package,²³ using the B3LYP exchange-correlation functional^{24,25} and a 6-311G* basis set for all atoms other than ruthenium, and the SRSC effective core potential (ECP)²⁶ for the core orbitals of the ruthenium atom. The N3 molecule geometry was optimized at this level of theory using an SCF (self consistent field) convergence criterion of 10^{-8} and a cutoff of 10^{-10} for the neglect of two electron integrals, and molecular orbitals were plotted using an isovalue of 0.04 electrons/bohr³. DFT calculations of the hydrogen bonding motif of bi-isonicotinic acid [Fig. 1(b)] included an empirical dispersion correction via the Grimme BJ-damping model DFT-D3(BJ).²⁷

III. RESULTS AND DISCUSSION

A. Isonicotinic acid

The N 1s RIXS map measured for the isonicotinic acid (see Fig. 1) crystalline powder is shown in Fig. 2. Elastic scattering gives rise to a narrow feature that disperses linearly in emission energy as the absorption energy increases. At an absorption energy of 398.6 eV, there is a strong enhancement in the intensity just below the elastic line and strong inelastic scattering features observed below ~ 395 eV emission energy. This absorption (A) is attributed to excitation from the N 1s core-level to the LUMO-derived state of the core-excited molecule. This is consistent with previous electron yield XAS measurements for multilayer films of isonicotinic acid deposited on titanium dioxide surfaces.^{13,14} The intensity observed to the low emission energy side of the elastic line does not disperse linearly with the elastic line but instead is observed at an almost constant emission energy of 398 eV. This corresponds to radiative decay of the core-hole always from the same vibrational component of the core-excited state. While the absorption energy is tuned over the LUMO-derived resonance (A), dissipation of the vibrational energy results in the decay proceeding from the lowest accessible state. This feature is therefore attributed to vibronic coupling.²⁸ The main feature of the inelastic scattering at resonance A is the strong enhancement of feature I at an emission energy of 393.6 eV. This is attributed to radiative decay from the highest occupied molecular orbital (HOMO). Weaker enhancements are observed at energies of 390.4 eV (II_A) and 387.5 eV (III) attributed to decay from lower energy molecular orbitals (the matrix element). The inelastic scattering represents the partial density of states of the molecule modulated by the coupling between the occupied and unoccupied molecular

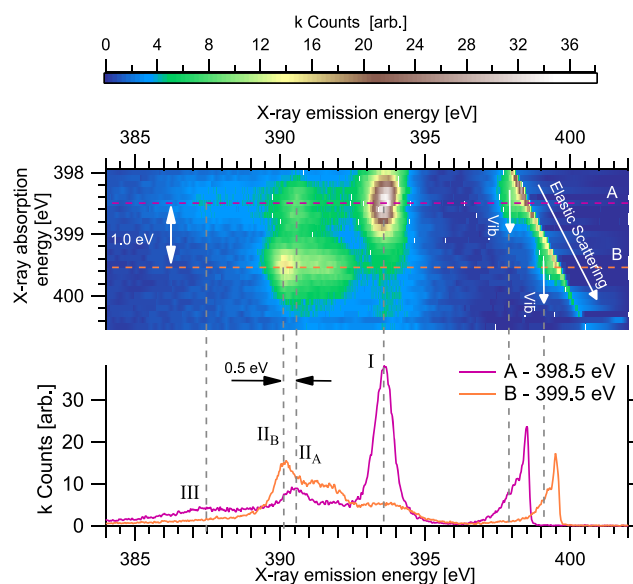


FIG. 2. N 1s RIXS map for the isonicotinic acid crystalline powder. The features observed below 397 eV emission energy are attributed to inelastic scattering and those above 397 eV emission energy to elastic (Rayleigh) scattering and small inelastic losses due to vibronic coupling (indicated by the downward arrows).

orbitals involved. The strong enhancement of peak I at resonance A is therefore attributed to strong coupling between the HOMO and the LUMO, while peaks II_A and III have a relatively weaker coupling with the LUMO.

At an absorption energy of 399.5 eV, a second band of enhancements (B) is observed both on the lower emission energy side of the elastic line and within the manifold of inelastic scattering. The intensity just below the elastic line is again attributed to vibronic coupling as for the LUMO. In this case, the vibronic emission is observed at an almost constant energy of 399.2 eV. The separation between the main absorption energy and the vibronic line is 0.3 eV for resonance B compared with 0.5 eV for resonance A. This difference is attributed to the different character of this molecular orbital, which is further illustrated by the inelastic scattering. At the absorption energy of resonance B, the strongest enhancement is observed at an emission energy of 390.2 eV (II_B) and a broad shoulder extending up to 391.2 eV. An absorption similar to resonance B has previously been observed in the electron yield XAS of multilayers of isonicotinic acid deposited on a titanium dioxide surface.^{13,14} This resonance was shown to be highly dependent on the growth conditions of the film and attributed to hydrogen-bonding between the carboxylic group of one molecule and the N atom of the pyridine ring of a neighboring molecule, which forms only when the molecules are deposited at a very slow rate. In the XAS multilayer studies^{13,14} the separation of resonances A and B was 1.2 eV, compared to 1.0 eV in the RIXS results shown in Fig. 2 for the crystalline powder. Since the crystal structure of isonicotinic acid is known to be hydrogen bonded,¹⁵ we attribute resonance B to a new LUMO state arising from this N···OH hydrogen bond interaction, with the small difference in energy likely due to the slightly different bonding environments in the bulk crystal compared with the physisorbed multilayer.

B. Bi-isonicotinic acid

The N 1s RIXS map measured for the bi-isonicotinic acid [see Fig. 1(a)] crystalline powder is shown in Fig. 3(a). The RIXS data for the bi-isonicotinic acid powder exhibit similar features to isonicotinic acid, which is largely expected due to the similarity of the molecular structures. We find the first absorption resonance at an absorption energy of 398.4 eV (A) where we again observe inelastic scattering involving the occupied molecular orbitals below an emission energy of around 395 eV. The strongest of these (I_A) appears at an emission energy of 393.5 eV attributed as for isonicotinic acid to the HOMO. Weaker features are observed at 390 eV (II_A) and 387 eV (III_A) attributed to decay from lower lying molecular orbitals. Resonance A is attributed to the LUMO and while this appears at a slightly different absorption energy compared to isonicotinic acid, we find the resulting inelastic scattering to bear a striking similarity with the single ring molecule.

At an absorption energy of 399.5 eV, a second band of enhancements (B) is observed both on the lower emission energy side of the elastic line and within the manifold of inelastic scattering. Similar to isonicotinic acid, we find a much weaker intensity for peak I_B. This peak is also shifted slightly to higher emission energy (394.0 eV). Peak II_B is observed at a similar intensity to II_A but shifted in the other direction to lower emission energy. We note that the II_A – II_B shift is 0.5 eV for both bi-isonicotinic and isonicotinic acids. The

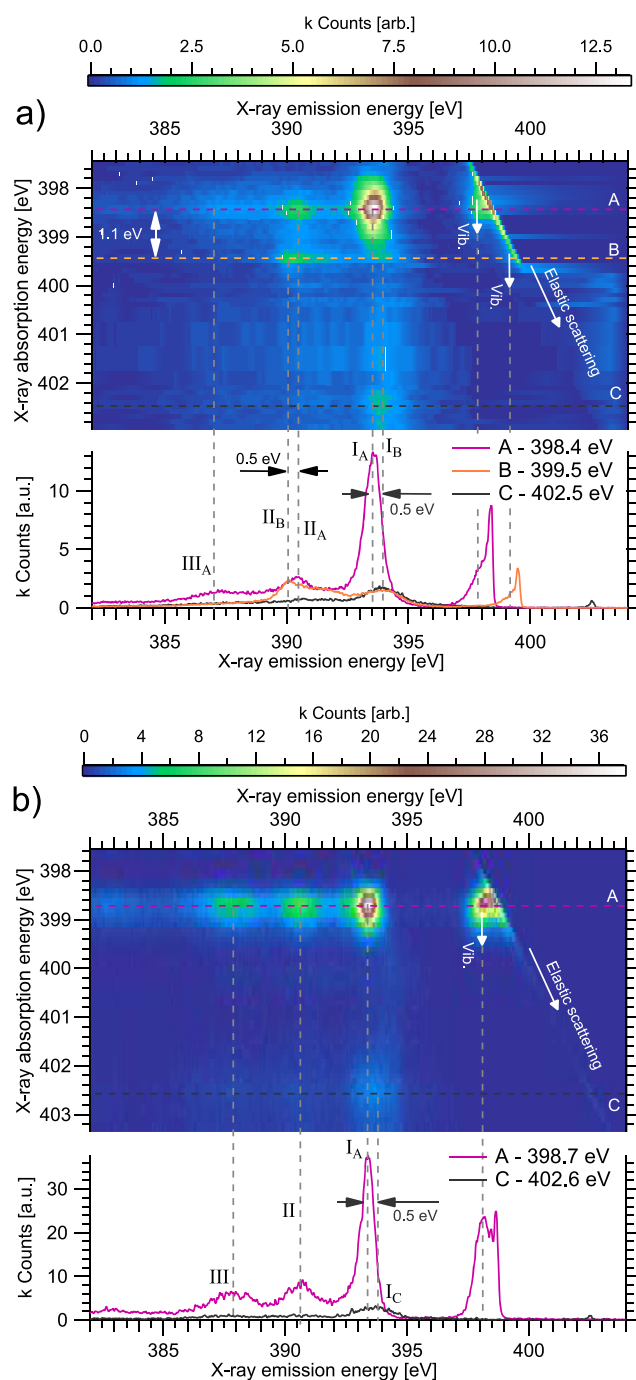


FIG. 3. Bi-isonicotinic acid N 1s RIXS maps of (a) crystalline powder and (b) physisorbed multilayer. The downward arrows mark vibronic coupling features. Line profiles have been extracted for key resonant transitions.

absorption energy separation of resonances A and B is ~ 1 eV which is consistent with the corresponding separation for isonicotinic acid, and we again attribute resonance B to intermolecular N···OH hydrogen bonding in the bulk crystalline powder. The next resonance,

labeled C, occurs at an absorption energy of 402.6 eV. This couples with a state at the same energy as the I_B feature centered at 394.0 eV.

The N 1s RIXS map measured for multilayer bi-isonicotinic acid physisorbed on TiO₂(110) is shown in Fig. 3(b). These data have been published previously²⁸ but is reproduced here in the same format as the powder data for direct comparison. Many spectral features are similar: the emission spectra on resonance A have features I, II, and III appearing at the same energies and both have the same 0.5 eV shift between the HOMO enhancement at the A and C resonances. The key difference between the powder and the multilayer is the absence of resonance B in the physisorbed multilayer. This we attribute to the lack of hydrogen bonding between the molecules in the multilayer prepared by thermal evaporation. This is consistent with XPS, XAS, and RPES measurements of bi-isonicotinic acid physisorbed multilayers where no evidence of hydrogen bonding has been observed.^{11,13} Compared to the powder sample, features II and III in the multilayer are also more intense relative to feature I. We attribute this difference to the additional molecular orbitals formed in the presence of hydrogen bonding, which inevitably impact the surrounding density of states.

For both the powder and the multilayer, the intensity observed at resonance A on the lower emission energy side of the elastic line is attributed to vibronic coupling (as for isonicotinic acid) which is discussed in detail elsewhere.²⁹ Here, we note that this relative intensity of the vibronic feature is much stronger for the multilayer compared with the bulk powder, where the vibronic coupling is most likely suppressed by the effect of the extended crystal structure mediated by the N...OH hydrogen bonding.

C. Ru photosensitizer “N3”

1. N3—Calculated molecular orbitals

The molecular orbital and electronic structure of the N3 molecule are well understood—for a thorough computational analysis, we would point the reader to the DFT study by Monat *et al.*³⁰ However, in order to aid discussion here, schematics showing localization of relevant molecular orbitals are included in Fig. 4. We would like to stress that these ground state DFT calculations are not intended to be an extensive simulation of the molecule’s electronic properties in the context of this experiment—important details such as the effects of the core-hole are not included—but the calculations are intended to give readers not familiar with the molecule an insight into the orbital localization.

The three occupied molecular orbitals shown in Fig. 4, orbital numbers 163 (HOMO), 158 and 156, are all good representations of the orbitals with nearby energies. Orbitals 163–160 are mainly localized on the thiocyanate ligands and Ru atom. For orbitals 159–157, we see some density start to shift to the bi-isonicotinic acid ligands. By orbital 156, the density is localized almost exclusively on the bi-isonicotinic acid. The LUMO (orbital 164) is largely localized on the bi-isonicotinic acid ligands and the Ru center. With the exception of the LUMO+1 (orbital 165), which is distributed over the entire molecule, we do not see any notable density on the thiocyanate ligand until we reach orbital 175. When we reach orbital 188, we see that the orbital is localized almost exclusively on the thiocyanate ligands.

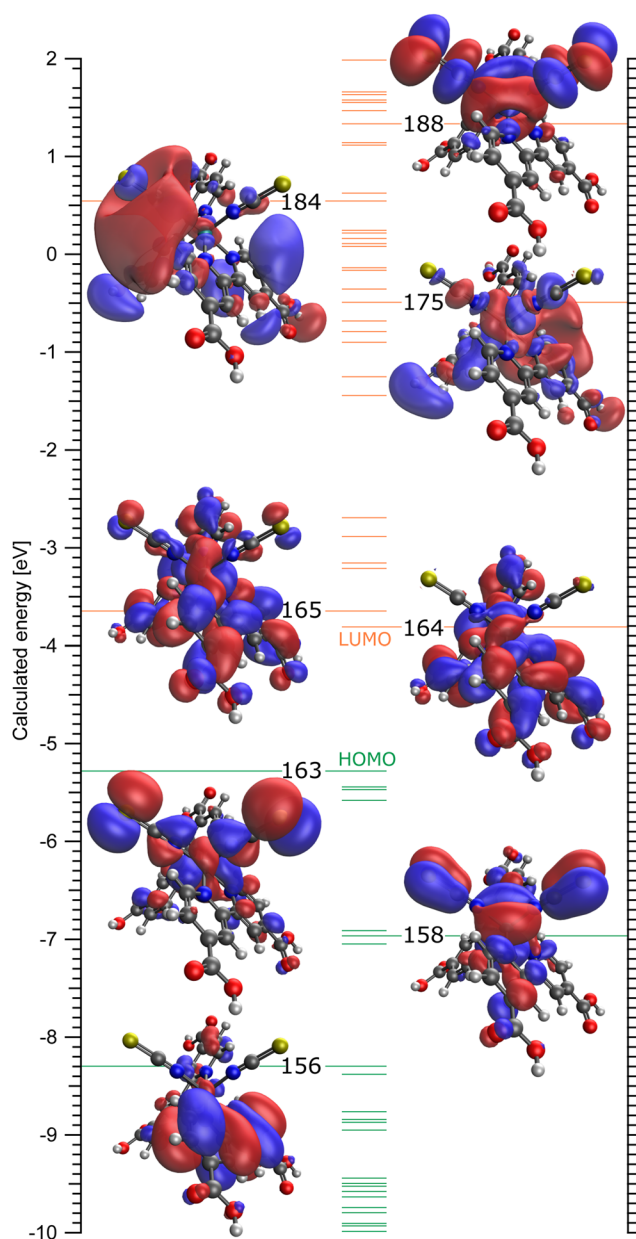


FIG. 4. Energies of occupied (green) and unoccupied (orange) molecular orbitals from ground state DFT calculations of an isolated N3 molecule. The localization of orbitals 156 (−8.30 eV), 158 (−6.97 eV), 163 (HOMO, −5.28 eV), 164 (LUMO, −3.81 eV), 164 (−3.65 eV), 175 (−0.49 eV), 184 (+0.54 eV), and 188 (+1.33 eV) is shown.

2. N3—RIXS data

The N 1s RIXS map measured for the N3 dye [see Fig. 1(a)] powder is shown in Fig. 5. The first resonance (A) representing excitation into the LUMO is observed at an absorption energy centered around 399.2 eV. The inelastic scattering at this resonance exhibits

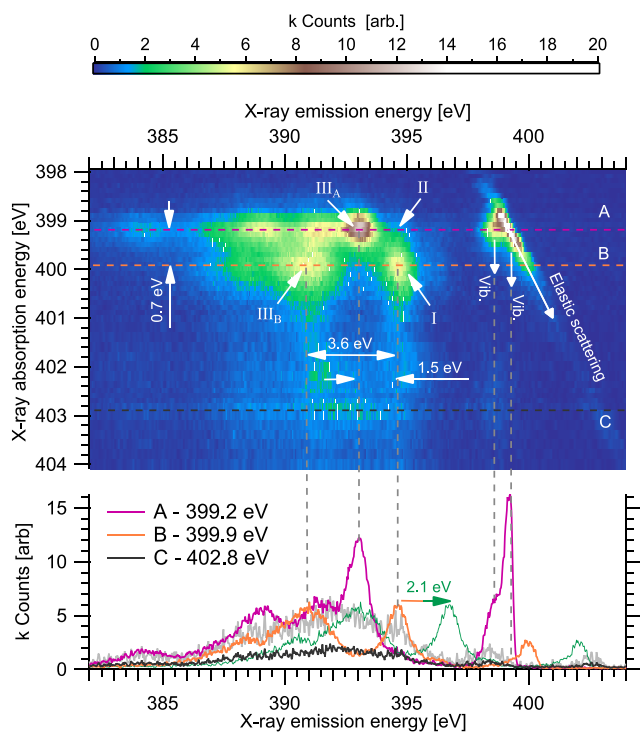


FIG. 5. N 1s RIXS of the N3 dye (bulk powder sample). Line profiles A (purple) and B (orange) have been extracted from the map and represent excitation of the nitrogen atoms in the bi-isonicotinic acid and thiocyanate ligands, respectively. Intensity attributed to vibronic coupling from the two ligands is indicated with the downward arrows. Line profile C (black) has also been extracted—the light gray line shows this with the intensity multiplied by 3. The green line shows profile B shifted by 2.1 eV (the binding energy difference between the two N 1s core levels).

a weak feature at 395 eV (II_A) emission energy and an intense feature at 393 eV (III_A), followed by a series of decreasing intensity peaks at 391, 389, and 384 eV. A second resonance (B) is observed to be 0.7 eV higher at 399.9 eV absorption energy. Here, we observe a feature at 395 eV (I) in the inelastic scattering, but effectively no intensity at the emission energy of feature III_A . The data also show a low intensity feature at emission energy ~ 394 eV—the higher energy side of feature I (on resonance B).

The intensity just below the elastic line at resonance A in the RIXS map is attributed, as for the isonicotinic and bi-isonicotinic acid molecules, to vibronic coupling and is observed at an almost constant emission energy of ~ 398.5 eV as the absorption is tuned over the LUMO-derived resonance. By the time resonance B is reached, the intensity of this feature is dramatically reduced and is barely visible in the line profile. However, looking at the elastic peak at 399.9 eV on line profile B, we see a shoulder on the lower emission energy side at ~ 398.5 eV. These two observations imply that resonance B is exciting into a molecular orbital that is completely distinct from the resonance A LUMO. Interestingly, the vibronic feature associated with the resonance A (bi-isonicotinic acid) LUMO reappears as a weak feature between ~ 402 eV and ~ 403.5 eV absorption energy (centered around absorption C at 402.8 eV). The inelastic

scattering in this region suggests that these unoccupied molecular orbitals are distributed across the whole molecule, exhibiting features characteristic of both resonances A and B. The vibronic feature, however, results from a core-hole decay process originating from the lowest vibrational state of the LUMO. For this feature to be observed for these higher-lying states, this could imply a two-step decay process where the photoexcited electron first decays from these higher unoccupied orbitals to the LUMO before filling the N 1s core-hole (in the time scale of the core-hole lifetime).

3. N3–RPES data

Further insight into the core-excited state of N3 can be obtained from the N 1s resonant photoemission (RPES), presented in Fig. 6. This technique is the nonradiative analog of RIXS and involves the same core-excited intermediate state. Also presented in Fig. 6 are direct photoemission spectra of the valence band of the N3 multilayer and the underlying $TiO_2(110)$ surface for comparison.

As discussed for the RIXS map, resonance B at an absorption energy of 399.8 eV is predominantly located on the thiocyanate ligands. Here, we observe a participator enhancement (I) at a binding energy of 2.5 eV. This corresponds to a resonant enhancement of the HOMO of N3. A second enhancement (III) is observed at this resonance at a binding energy of 6.1 eV. The separation of 3.6 eV is identical to that presented in the RIXS (Fig. 5) supporting our assignment of this feature.

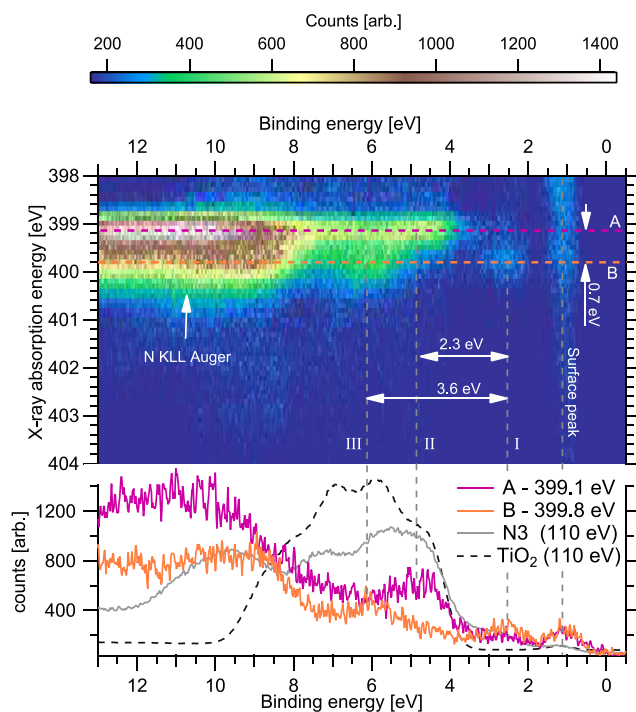


FIG. 6. N 1s RPES for an N3 multilayer. Line profiles A and B are again extracted representing excitation into the bi-isonicotinic acid and NCS ligands. These are compared to valence band XPS of the same sample of N3 (solid gray line) and the clean titanium dioxide surface (dashed black line). Features I, II, and III are attributed to the same occupied molecular orbitals responsible for the corresponding features highlighted in the RIXS (Fig. 5).

Resonance A—attributed largely to the bi-isonicotinic acid ligands—is observed at an absorption energy of 399.1 eV. Here, we observe only a weak resonant enhancement of the HOMO at a binding energy of 2.5 eV (I) and a stronger enhancement of a broad feature centered just below 5 eV (2.3 eV below the HOMO). This feature (II) is attributed to the next experimentally distinct occupied molecular orbital. This feature is not enhanced at resonance B, suggesting that this orbital is localized on the bi-isonicotinic acid ligands. Returning to the RIXS map (Fig. 5), we can now associate the weak intensity observed at 395 eV at resonance A (feature II) with this same occupied orbital.

The vertical, constant binding energy bands of intensity observed in the N 1s RPES map in Fig. 6 are due to direct photoemission of the valence states of the molecule and the underlying surface and contribute only to a background of slowly decreasing intensity (due to decreasing cross section with increasing photon energy). Our assignments of molecule and surface features are consistent with valence band XPS (measured at 110 eV photon energy) of the N3 deposit and the underlying clean TiO₂(110) surface which are included in Fig. 6 for reference. The structure of the surface valence band matches well with the preabsorption edge features visible in the map.

4. N3—discussion

We first note that N···OH hydrogen bonding is not possible for the N3 dye complex as all the nitrogen atoms are bonded to the central ruthenium atom. Therefore, resonance B, unlike isonicotinic and bi-isonicotinic acid, cannot be attributed to intermolecular hydrogen bonding. Feature I is not observed at all in the RIXS of bi-isonicotinic acid and is assigned to the HOMO of N3. As shown by our DFT calculations (Fig. 4), the HOMO is located predominantly on the thiocyanate ligands, while the LUMO is located largely on the bi-isonicotinic acid ligand. We would therefore expect a weak coupling to the HOMO at the LUMO-resonance (A), which is consistent with the RIXS and RPES maps. Resonance B, on the other hand, is therefore attributed to excitation into higher unoccupied molecular orbitals localized largely on the thiocyanate ligands.

In the DFT, we do not see substantial density appearing on the thiocyanate until we reach orbital 184 and 4.35 eV above the LUMO. However, in the RIXS and RPES, we see a separation of 0.7 eV between the two resonances. This can be understood by considering that the resonant transitions are dependent on the energy of both the core level and the unoccupied level. Core-level photoemission spectroscopy of N3 has shown that the N 1s environment in the thiocyanate appears 2.1 eV lower in binding energy than that in the pyridine ring of the bi-isonicotinic acid ligand.⁵ Therefore, the experimental data imply that the unoccupied molecular orbitals on the thiocyanate actually lie 0.7 eV + 2.1 eV = 2.8 eV above the LUMO. Although this is still lower than the calculated separation, one has to remember that the experiments measure decay processes from a core-excited state—the effects of the core-hole should be considered carefully if one wanted to precisely simulate X-ray absorption experiments.

For resonant photoemission (RPES), interpretation of the binding energy axis is trivial as it is not dependent on the photon or core-level energies—participator decay in RPES leaves the atom in a final state identical to that of normal photoemission of the

occupied molecular orbital. For RIXS however, the measured photon is produced by filling the core hole—the binding energy of which therefore needs to be considered. In this case, the RIXS spectra are therefore a projection of the molecule's partial density of states onto the two different nitrogen core level environments, so we again need to consider the 2.1 eV energy difference between these core levels. The separation of peaks I and III_A in the RIXS map is 1.5 eV emission energy, which therefore translates into a binding energy difference of 3.6 eV. This is consistent with the separation of the features in the valence band photoemission, shown in Fig. 6, which supports this interpretation. Moreover, if peak III_B (in the RIXS) is shifted to higher emission energy by 2.1 eV as required by this interpretation (shown in Fig. 5), its emission energy coincides with peak III_A identifying both peaks as the same occupied molecular orbital. This can also be realized by the observation that the emission energy separation of peaks I and III_B is indeed 3.6 eV.

The features attributed to experimentally distinct occupied molecular orbitals (I, II, and III) match well with the first three groupings of calculated occupied molecular orbitals (see Fig. 4), represented by orbitals 163 (HOMO), 158, and 156. Specifically, orbitals 158 and 156 appear 1.7 eV and 3.0 eV below the HOMO, respectively, which is a close match in relative energies considering the nature of the calculations.

Despite the complexities in the analysis of the RIXS where the core-level needs to be considered, we are still able to compare the shape of the emission spectra measured on the LUMO resonance for all three molecules relative to the HOMO on the pyridine (differences in core level positions would manifest as a shift in emission energy). This is presented in Fig. 7 with the spectra normalized to the pyridine HOMO, the energy of which also defines “0 eV.” When comparing the isonicotinic acid and bi-isonicotinic powders, we see very similar structures. This is not surprising given the similarity of the two molecules. However, when compared to the N3, we see that although the ligand is the same, the electronic structure is very different; the features are broader and appear at different relative energies. Again, this is not surprising as the environment is very different (the nitrogen has an additional ruthenium bond). This shows that one has to take great care when using N 1s based transitions in

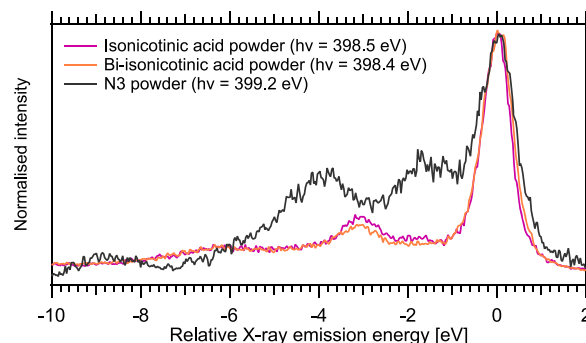


FIG. 7. N 1s RIXS emission spectra for all three powder samples measured on the LUMO resonances. The energy axis is relative to the position of the pyridine nitrogen's HOMO. Spectra are normalized to the height of this HOMO.

bi-isonicotinic acid as a model system for N3, or similar complexes with this common anchoring ligand. It also highlights the value of RIXS to study these systems. Despite the much simpler binding energy axis in RPES, making this type of comparison would be much more challenging due to the strong N KLL Auger feature that overlaps the participant enhancements of the molecular orbitals, especially when considering weak features ~ 10 eV below the HOMO.

IV. CONCLUSIONS

We have measured N 1s RIXS maps of the dye molecule *cis*-bis(isothiocyanato) bis(2,2'-bipyridyl-4,4'-dicarboxylic acid) ruthenium(II) and of the isolated ligand bi-isonicotinic acid and the single ring analog isonicotinic acid in the bulk powder. For both the isonicotinic and bi-isonicotinic acids in the bulk crystalline powder form, we see direct evidence of hydrogen bonding in the form of a resonant transition at 399.5 eV absorption energy. This assignment was aided by comparison to a physisorbed multilayer where hydrogen bonding is not present. For the bulk powder, we also see evidence of vibronic coupling but note that the features are less intense than observed in the multilayer. For the N3 dye complex, we interpret the RIXS in terms of the orbital contributions of the bi-isonicotinic acid and thiocyanate ligands and the projection of the partial densities of states onto the different nitrogen atoms. Further interpretation is provided through comparison with resonant photoemission spectroscopy (RPES) and density functional theory (DFT) calculations highlighting the usefulness of combining these three complementary techniques for understanding the electronic structure of complex molecules. This analysis allowed us to confirm the localization and relative coupling of the frontier orbitals and associated vibrational losses for this important photosensitizer complex. Comparison of the X-ray emission spectra of the bi-isonicotinic acid ligand in N3 to those of the isolated ligands highlights that care needs to be taken when using isolated ligands as model systems for these complex dye molecules.

ACKNOWLEDGMENTS

We are grateful to the authors of Ref. 3 for access to the RPES data presented in Fig. 6. Experiments were funded by RCUK Engineering and Physical Sciences Research Council (EPSRC) and MolecularSpray Ltd. through a DTG/CASE conversion studentship, and the European Community's Seventh Framework Programme (Grant No. FP7/2007-2013) CALIPSO under Grant Agreement No. 312284.

REFERENCES

- ¹M. Grätzel, *J. Photochem. Photobiol.*, **C 4**, 145 (2003).
- ²J. J. Concepcion, J. W. Jurss, M. K. Brennaman, P. G. Hoertz, A. O. T. Patrocinio, N. Y. Murakami Iha, J. L. Templeton, and T. J. Meyer, *Acc. Chem. Res.* **42**, 1954 (2009).
- ³L. C. Mayor, J. Ben Taylor, G. Magnano, A. Rienzo, C. J. Satterley, J. N. O'Shea, and J. Schnadt, *J. Chem. Phys.* **129**, 114701 (2008).
- ⁴L. C. Mayor, A. Saywell, G. Magnano, C. J. Satterley, J. Schnadt, and J. N. O'Shea, *J. Chem. Phys.* **130**, 164704 (2009).
- ⁵A. J. Britton, M. Weston, J. B. Taylor, A. Rienzo, L. C. Mayor, and J. N. O'Shea, *J. Chem. Phys.* **135**, 164702 (2011).
- ⁶A. J. Gibson, R. H. Temperton, K. Handrup, M. Weston, L. C. Mayor, and J. N. O'Shea, *J. Chem. Phys.* **140**, 234708 (2014); e-print arXiv:1407.5186.
- ⁷J. B. Taylor, L. C. Mayor, J. C. Swarbrick, J. N. O'Shea, C. Isvoranu, and J. Schnadt, *J. Chem. Phys.* **127**, 134707 (2007).
- ⁸L. Patthey, H. Rensmo, P. Persson, K. Westermark, L. Vayssieres, A. Stashans, A. Petersson, P. A. Bruhwiler, H. Siegbahn, S. Lunell, and N. Martensson, *J. Chem. Phys.* **110**, 5913 (1999).
- ⁹P. Persson, S. Lunell, P. A. Bruhwiler, J. Schnadt, S. Södergren, J. N. O'Shea, O. Karis, H. Siegbahn, N. Mårtensson, M. Bässler, and L. Patthey, *J. Chem. Phys.* **112**, 3945 (2000).
- ¹⁰J. Schnadt, A. Henningsson, M. P. Andersson, P. G. Karlsson, P. Uvdal, H. Siegbahn, P. A. Bruhwiler, and A. Sandell, *J. Phys. Chem. B* **108**, 3114 (2004).
- ¹¹R. Temperton, A. Gibson, K. Handrup, and J. O'Shea, *J. Chem. Phys.* **147**, 054703 (2017).
- ¹²E. Tynan, P. Jensen, P. E. Kruger, A. C. Lees, and M. Nieuwenhuizen, *Dalton Trans.* **117**, 1223 (2003).
- ¹³J. O'Shea, Y. Luo, J. Schnadt, L. Patthey, H. Hillesheimer, J. Krempasky, D. Nordlund, M. Nagasono, P. Bruhwiler, and N. Mårtensson, *Surf. Sci.* **486**, 157 (2001).
- ¹⁴J. N. O'Shea, J. Schnadt, P. A. Bruhwiler, H. Hillesheimer, N. Mårtensson, L. Patthey, J. Krempasky, C. Wang, Y. Luo, and H. Ågren, *J. Phys. Chem. B* **105**, 1917 (2001).
- ¹⁵F. Takusagawa and A. Shimada, *Acta Crystallogr., Sect. B: Struct. Crystallogr. Cryst. Chem.* **32**, 1925 (1976).
- ¹⁶T. Schmitt, F. M. F. de Groot, and J.-E. Rubensson, *J. Synchrotron Radiat.* **21**, 1065 (2014).
- ¹⁷C. S. Ponceca, P. Chábera, J. Uhlig, P. Persson, and V. Sundström, *Chem. Rev.* **117**, 10940 (2017).
- ¹⁸V. Vaz da Cruz, F. Gel'mukhanov, S. Eckert, M. Iannuzzi, E. Ertan, A. Pietzsch, R. C. Couto, J. Niskanen, M. Fondell, M. Dantz, T. Schmitt, X. Lu, D. McNally, R. M. Jay, V. Kimberg, A. Föhlisch, and M. Odelius, *Nat. Commun.* **10**, 1013 (2019).
- ¹⁹L. Weinhardt, E. Ertan, M. Iannuzzi, M. Weigand, O. Fuchs, M. Bär, M. Blum, J. D. Denlinger, W. Yang, E. Umbach, M. Odelius, and C. Heske, *Phys. Chem. Chem. Phys.* **17**, 27145 (2015).
- ²⁰S. G. Chiuzaian, C. F. Hague, A. Avila, R. Delaunay, N. Jaouen, M. Sacchi, F. Polack, M. Thomasset, B. Lagarde, A. Nicolau, S. Brignolo, C. Baumier, J. Lüning, and J. M. Mariot, *Rev. Sci. Instrum.* **85**, 043108 (2014).
- ²¹M. Sacchi, N. Jaouen, H. Popescu, R. Gaudemer, J. M. Tonnerre, S. G. Chiuzaian, C. F. Hague, A. Delmotte, J. M. Dubuisson, G. Cauchon, B. Lagarde, and F. Polack, *J. Phys.: Conf. Ser.* **425**, 072018 (2013).
- ²²R. H. Temperton, J. N. O'Shea, and D. J. Scurr, *Chem. Phys. Lett.* **682**, 15 (2017).
- ²³Y. Shao, Z. Gan, E. Epifanovsky, A. T. Gilbert, M. Wormit, J. Kussmann, A. W. Lange, A. Behn, J. Deng, X. Feng, D. Ghosh, M. Goldey, P. R. Horn, L. D. Jacobson, I. Kaliman, R. Z. Khaliullin, T. Kus, A. Landau, J. Liu, E. I. Proynov, Y. M. Rhee, R. M. Richard, M. A. Rohrdanz, R. P. Steele, E. J. Sundstrom, H. L. Woodcock, P. M. Zimmerman, D. Zuev, B. Albrecht, E. Alguire, B. Austin, G. J. O. Beran, Y. A. Bernard, E. Berquist, K. Brandhorst, K. B. Bravaya, S. T. Brown, D. Casanova, C.-M. Chang, Y. Chen, S. H. Chien, K. D. Closser, D. L. Crittenden, M. Diedenhofen, R. A. DiStasio, H. Do, A. D. Dutoi, R. G. Edgar, S. Fatehi, L. Fusti-Molnar, A. Ghysels, A. Golubeva-Zadorozhnaya, J. Gomes, M. W. Hanson-Heine, P. H. Harbach, A. W. Hauser, E. G. Hohenstein, Z. C. Holden, T.-C. Jagau, H. Ji, B. Kaduk, K. Khistyayev, J. Kim, J. Kim, R. A. King, P. Klunzinger, D. Kosenkov, T. Kowalczyk, C. M. Krauter, K. U. Lao, A. D. Laurent, K. V. Lawler, S. V. Levchenko, C. Y. Lin, F. Liu, E. Livshits, R. C. Lochan, A. Luenser, P. Manohar, S. F. Manzer, S.-P. Mao, N. Mardirossian, A. V. Marenich, S. A. Maurer, N. J. Mayhall, E. Neuscamman, C. M. Oana, R. Olivares-Amaya, D. P. O'Neill, J. A. Parkhill, T. M. Perrine, R. Peverati, A. Prociuk, D. R. Rehn, E. Rosta, N. J. Russ, S. M. Sharada, S. Sharma, D. W. Small, A. Sodt, T. Stein, D. Stück, Y.-C. Su, A. J. Thom, T. Tsuchimochi, V. Vanovschi, L. Vogt, O. Vydrov, T. Wang, M. A. Watson, J. Wenzel, A. White, C. F. Williams, J. Yang, S. Yeganeh, S. R. Yost, Z.-Q. You, I. Y. Zhang, X. Zhang, Y. Zhao, B. R. Brooks, G. K. Chan, D. M. Chipman, C. J. Cramer, W. A. Goddard, M. S. Gordon, W. J. Hehre, A. Klant, H. F. Schaefer, M. W. Schmidt, C. D. Sherrill, D. G. Truhlar, A. Warshel, X. Xu, A. Aspuru-Guzik, R. Baer, A. T. Bell, N. A. Besley, J.-D. Chai, A. Dreuw,

- B. D. Dunietz, T. R. Furlani, S. R. Gwaltney, C.-P. Hsu, Y. Jung, J. Kong, D. S. Lambrecht, W. Liang, C. Ochsenfeld, V. A. Rassolov, L. V. Slipchenko, J. E. Subotnik, T. Van Voorhis, J. M. Herbert, A. I. Krylov, P. M. Gill, and M. Head-Gordon, *Mol. Phys.* **113**, 184 (2015).
- ²⁴A. D. Becke, *J. Chem. Phys.* **98**, 5648 (1993).
- ²⁵P. J. Stephens, F. J. Devlin, C. F. Chabalowski, and M. J. Frisch, *J. Phys. Chem.* **98**, 11623 (1994).
- ²⁶D. Andrae, U. Häußermann, M. Dolg, H. Stoll, and H. Preuß, *Theor. Chim. Acta* **77**, 123 (1990).
- ²⁷S. Grimme, S. Ehrlich, and L. Goerigk, *J. Comput. Chem.* **32**, 1456 (2011).
- ²⁸J. N. O'Shea, K. Handrup, R. H. Temperton, A. J. Gibson, A. Nicolaou, and N. Jaouen, *J. Chem. Phys.* **147**, 134705 (2017).
- ²⁹J. N. O'Shea, K. Handrup, R. H. Temperton, A. J. Gibson, A. Nicolaou, N. Jaouen, J. B. Taylor, L. C. Mayor, J. C. Swarbrick, and J. Schnadt, *J. Chem. Phys.* **148**, 204705 (2018).
- ³⁰J. E. Monat, J. H. Rodriguez, and J. K. McCusker, *J. Phys. Chem. A* **106**, 7399 (2002).